International Journal of Concrete Structures and Materials
Vol.11, No.2, pp.285–300, June 2017
DOI 10.1007/s40069-017-0192-9
ISSN 1976-0485 / eISSN 2234-1315

Seismic Capacity Design and Retrofit of Reinforced Concrete Staggered Wall Structures

Jinkoo Kim[1),*], and Younghoo Choi[2)]

(Received April 13, 2016, Accepted January 31, 2017, Published online May 19, 2017)

Abstract: This study investigates the seismic performance of a staggered wall structure designed with conventional strength based design, and compares it with the performance of the structure designed by capacity design procedure which ensures strong column-weak beam concept. Then the seismic reinforcement schemes such as addition of interior columns or insertion of rotational friction dampers at the ends of connecting beams are validated by comparing their seismic performances with those of the standard model structure. Fragility analysis shows that the probability to reach the dynamic instability is highest in the strength designed structure and is lowest in the structure with friction dampers. It is also observed that, at least for the specific model structures considered in this study, R factor of 5.0 can be used in the seismic design of staggered wall structures with proposed retrofit schemes, while R factor of 3.0 may be reasonable for standard staggered wall structures.

Keywords: staggered wall structures, seismic performance, capacity design, friction dampers.

1. Introduction

Reinforced concrete (RC) buildings having vertical shear walls both as partition walls and as load resisting systems have advantage in economic use of structural materials and ease of construction using slip forms. The seismic performance of RC shear wall structures have been widely investigated by many researchers (Wallace 2012; Kim 2016). The shear walls are also effective in preventing spread of fire (Kang et al. 2016). However the buildings with shear partition walls are not preferred these days mainly because the plan layouts fixed by the shear walls fail to meet the demand of people who prefer spatial variability. A staggered wall structure has story-high walls placed at alternate levels, which makes the system easier to remodel and consequently more sustainable while the economy and constructability of shear wall structures still maintained. Fintel (1968) proposed a staggered system for RC buildings in which staggered walls with attached slabs resist the gravity as well as the lateral loads as H-shaped story-high deep beams, and observed that the staggered wall systems would be more economical. Mee et al. (1975) investigated the structural performance of staggered wall systems by carrying out shaking table tests of 1/15 scaled models. Lee and Kim (2013) investigated the seismic performance of staggered wall structures with middle corridor; Kim and Baek (2013) conducted seismic risk assessment of staggered wall system structures; and Kim and Lee (2014) proposed a formula for fundamental natural period of staggered wall structures. Recently seismic behavior factors of the system were investigated based on the procedure recommended in the FEMA P 695 (2009) (Lee and Kim 2013, 2015), and ATC 19 (1995) (Kim et al. 2016). The seismic performance of a similar structure system in steel, the staggered truss system, has already been investigated (Kim et al. 2015; Kim and Kim 2017), and the system has been applied in many real building projects.

The staggered wall systems, however, have not been widely applied in practice due mainly to the lack of knowledge in the structural performance of the system. This study investigates the seismic performance of a staggered wall structure designed with conventional strength based design, and compares it with the performance of the structure design by capacity procedure which intends to ensure strong column-weak beam behavior. Then the seismic reinforcement schemes such as addition of interior columns or insertion of rotational friction dampers at the ends of connecting beams are implemented using the capacity design procedure. Their effects on enhancing seismic load-resisting capacity are validated by comparing their seismic performances with those of the standard model structure.

[1)]Department of Civil and Architectural Engineering, Sungkyunkwan University, Suwon, Korea.
*Corresponding Author; E-mail: jkim12@skku.edu
[2)]MCS-st Structural Engineering, Seoul, Korea.

2. Application of Energy Dissipation Devices in Shear Wall Structures

Even though there is no known example of a staggered wall structure with energy dissipation devices, many

researchers have been investigating the possibility of mitigating seismic response of structures with shear walls using dampers. Madsen et al. (2003) investigated the seismic performance of viscoelastic damping systems placed between shear walls at the coupling beam locations. Finite element methods were used to analyze the effects of dampers in these structural systems under different earthquakes records. The results of the analysis of the 20-storey structure with dampers in all levels illustrated that dampers could be used to improve the mitigation of seismic forces. Chung et al. (2009) proposed a friction damper that was applied between coupled shear walls in order to reduce the deformation of the structure induced by earthquake loads. It was found that the control performance of the proposed friction damper was superior to that of a coupled wall with a rigid beam. Mao et al. (2012) proposed a shape memory alloy (SMA) damper to be located in the middle of a coupling beam in a coupled shear wall building. In this study it was intended that, after earthquakes, deformation of the dampers can recover automatically because of the pseudoelasticity of austenite SMA material. Nonlinear time history analysis was conducted for an 18-story frame-shear wall structure with such SMA dampers to verify seismic response control effect of this damper. MacKay-Lyons (2013) developed the viscoelastic coupling damper (VCD) for RC coupled wall high-rise buildings. These dampers were introduced in place of coupling beams to provide distributed supplemental damping in all lateral modes of vibration. A parametric study has been conducted to determine the optimal number and placement of the dampers to achieve enhanced seismic performance. Results highlight the improved performance of VCDs over RC coupling beams at all levels of seismic hazard. Pant et al. (2015) developed viscoelastic coupling dampers to be located at coupling beams between two shear walls and at outrigger beams. They applied the system to a 40-story RC structure and found that the viscoelastic coupling dampers can be effective in reducing both structural and nonstructural damage under MCE level seismic events. The research results presented above confirm the effectiveness of energy dissipation devices in the design of shear wall structures.

3. Seismic Performance of Staggered Wall Structures

3.1 Configuration and Design of Staggered Wall Structures

In a typical staggered wall structure, the story-high RC walls that span the width of the building are located along the short direction in a staggered pattern. Figures 1 and 2 show the overall configuration and the structural plan of the 8-story example model structure, respectively, with 6 m long staggered walls along the transverse direction and moment frames located along the longitudinal direction. The two staggered walls at both sides of the middle corridor are connected with a 600 mm deep connecting beam. The thickness of the staggered walls is 200 mm throughout the stories. The staggered walls act like deep beams with the depth of a story height, and are reinforced with vertical and horizontal re-bars with diameter of 13 at 400 mm interval. The horizontal shear force delivered from staggered walls flows to the columns and staggered walls located below through the 210 mm thick floor diaphragm.

In this section the seismic performance of the model structure designed following the strength-based design procedure currently specified in design codes is evaluated. In this approach the structural members of the model structure are designed in such a way that the ratio of the member force demand to the design strength is maintained to be 0.8–0.9 for combined gravity and seismic loads. The dead and live loads are 7 and 2 kN/m^2, respectively, and the design seismic load is obtained using the seismic coefficients for short (S_{DS}) and 1.0 s period (S_{D1}) of 0.5 and 0.2, respectively, in the ASCE 7-13 (2013) format. The site class is assumed to be *C* and the response modification factor of 3.0 is used. The fundamental natural period of the model structure along the transverse direction is computed to be 0.40 s. Table 1 shows the size and rebar placement for the columns and the connection beams in the first story of the analysis model structure. The X shaped shear reinforcement composed of eight D13 rebars is provided in the connecting beams as shown in Fig. 3 to prevent shear failure prior to bending failure.

3.2 Analysis Modeling of the Structure

The staggered walls are modeled as deep beams using the General Wall fiber elements provided in the PERFORM 3D (2006) as shown in Fig. 4. The stress–strain material model of Paulay and Priestley (1992) is used for concrete as shown in Fig. 5a, in which the ultimate and yield strengths of concrete are 24 and 14 MPa, respectively, and the residual strength is defined as 20% of the ultimate strength. The strain at the ultimate strength is 0.002, and the ultimate strain is defined as 0.004. The reinforcing steel is modeled with bi-linear force–deformation relationship with the ultimate strength of 400 MPa as shown in Fig. 5b. The shear stress–strain relationship of the staggered wall is modelled by bi-linear lines with yield and ultimate strains of 0.004 and 0.012 respectively. Overstrength factors of 1.5 and 1.25 are used for concrete and reinforcing steel, respectively, in the nonlinear static and dynamic analyses.

Fig. 1 Schematic view of a staggered wall structure with middle corridor.

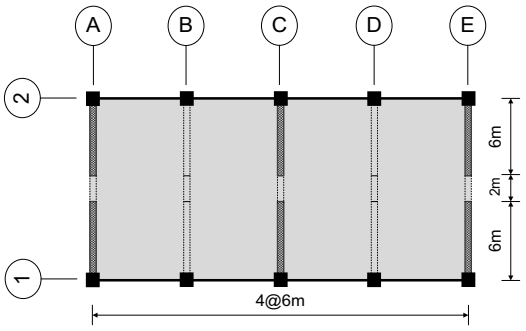

(a)

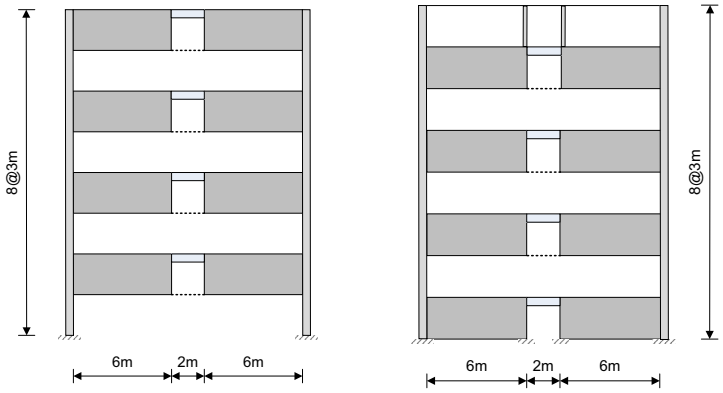

(b)

Fig. 2 Structural plan and elevation of the analysis model structure. **a** Structural plan and **b** elevation.

Table 1 Member size and rebars of the first story exterior columns.

Model	Frame	Size (mm)	Main rebars
SD	A	560 × 560	8-D25
	B	660 × 660	8-D29
CD	A	580 × 580	8-D29
	B	680 × 680	8-D32
CD_IC	A	540 × 540	8-D29
	B	640 × 640	8-D29
CD_FD	A	580 × 580	8-D29
	B	680 × 680	8-D32

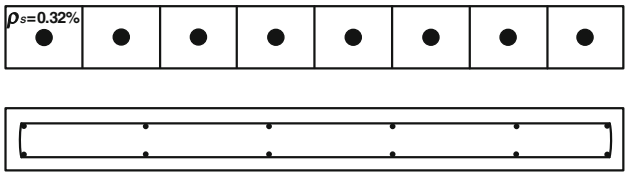

Fig. 4 Auto-sized fiber section for wall elements.

Nonlinear behavior of the RC columns located along the perimeter in the longitudinal direction is modeled using the 'FEMA Column, Concrete Type' element in Perform 3D developed based on an interpretation of the ASCE/SEI 41-13 (2013) Table 10-8. The nonlinear force–deformation relationships are shown in Figs. 6 and 7. To define a column plastic hinge, a moment-axial capacity interaction curve is

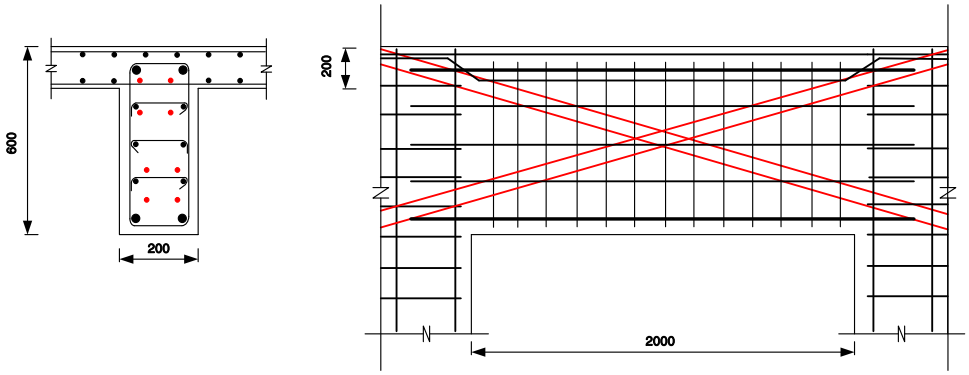

Fig. 3 X-shape rebars in the connecting beams.

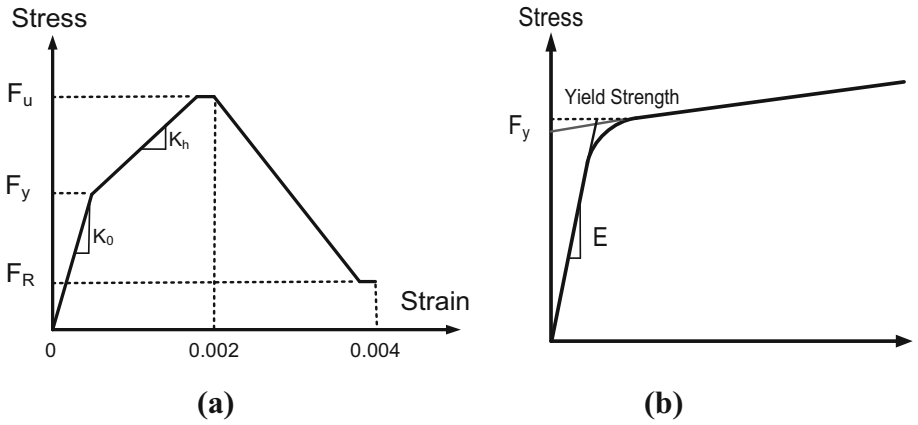

Fig. 5 Nonlinear models for reinforced concrete. **a** Concrete and **b** reinforcing steel.

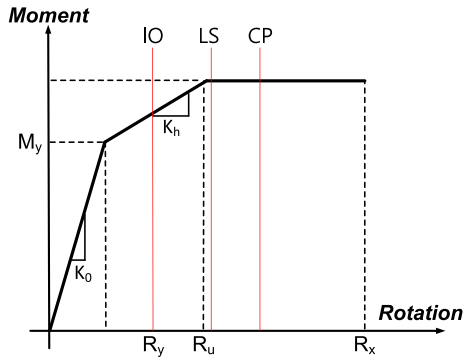

Fig. 6 Nonlinear model for columns.

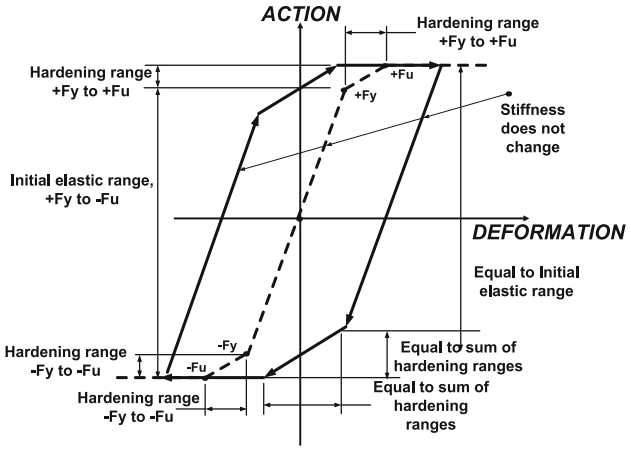

Fig. 7 Hysteresis loop of columns provided in the Perform 3D.

calculated using the expected material properties. The limit states defined in the ASCE/SEI 41-13 such as immediate occupancy (IO), life safety (LS), and collapse prevention (CP) are indicated in the curve. The back bone curve is tri-linear and M_y is assumed to be 80% of M_u. The unloading stiffness was modeled to be equal to the initial elastic stiffness. The energy degradation factor was set to be zero, which results in the same unloading and reloading lines. The analysis model for connecting beams located between the two staggered walls are composed of two end rotation type moment hinges and a middle shear hinge as shown in Fig. 8.

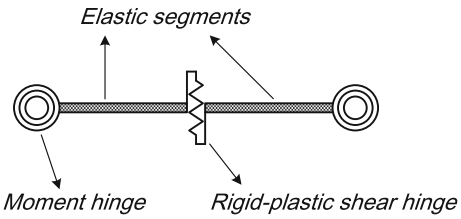

Fig. 8 Modeling of connecting beams.

Figure 9 shows the nonlinear model for connecting beams defined in ASCE/SEI 41-13.

3.3 Seismic Performance of the Strength-Designed Structure

To investigate the seismic performance and the collapse mode of the model structure, pushover analysis is carried out with the lateral load gradually increased proportional to the fundamental vibration mode shape vector. Figure 10 depicts the pushover curve which presents the base shear–roof displacement relationship of the model structure. The points of major plastic hinge formations and the maximum inter-story drift of 2.5% are marked on the pushover curve. It is noticed that plastic hinges occur first at the 5th story connecting beams. After reaching the maximum strength, the strength drops abruptly due to the formation of plastic hinges at the 5th story columns. Further strength drop occurs due to formation of plastic hinges at the 4th story columns. It can be observed that the maximum roof drift of the model structure at the major strength drop is significantly smaller than that of the structure at the maximum allowable inter-story drift of 2.5%. This implies that the strength-designed structure may not have enough ductility to satisfy the required seismic performance. Figure 11 shows the plastic hinge formation in an exterior frame and the adjacent interior frame at the maximum inter-story drift of 2% of the story height. The magnitude of the plastic rotation is also indicated as a percentage of the rotation corresponding to the CP state. It can be observed that many plastic hinges exceeding CP state form at the upper story columns and the plastic deformations in the connecting beams are relatively small. Based on the observation, it can be concluded that a typical staggered wall structure designed by current design code behaves as a

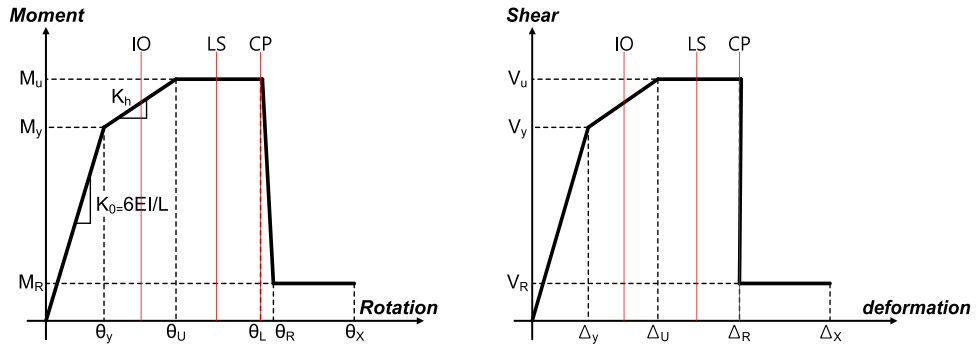

Fig. 9 Nonlinear model for connecting beams. **a** Moment–rotation relationship and **b** shear force–deformation relationship.

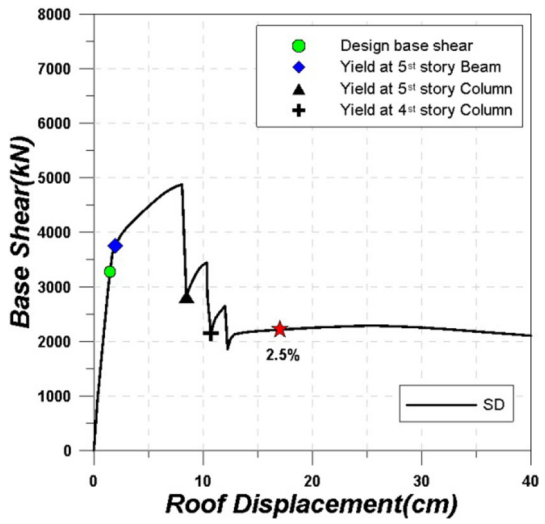

Fig. 10 Pushover curve of the strength-designed structure.

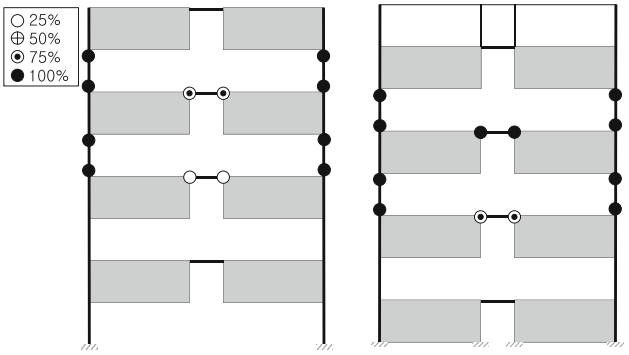

Fig. 11 Plastic hinge formation in the strength-designed structure at the maximum inter-story drift ratio of 2%.

strong beam weak column system when it is subjected to a seismic load.

4. Capacity Design Procedure

It is observed in the previous section that structural damage is concentrated in the exterior columns rather than in the connecting beams in the staggered wall structure designed following the code-based approach. In this section a capacity design procedure is applied to achieve the strong column-weak beam design of the model structure so that the damage in columns and the brittle failure mode observed in the conventional design are prevented. To this end the model structure is designed in such a way that the plastic hinges are concentrated at the connecting beams while the other members remain elastic. Similar approach has been successfully applied to the design of special truss moment frames by Chao and Goel (2006), who designed the special segment in the truss girders using the plastic design procedure. The design process was adopted to the AISC Seismic Provisions (2010).

The capacity design of the staggered wall system starts from the design of the connecting beams based on their required flexural strength at the ends. The target deformation is set to be 2% of the story height in each story. The target deformed shape and the desired plastic hinge formation are depicted in Fig. 12. The required total bending capacity of plastic hinges formed at the end of the connecting beams, $\sum_{i=1}^{m} M_{pi}$, can be calculated from the following equilibrium

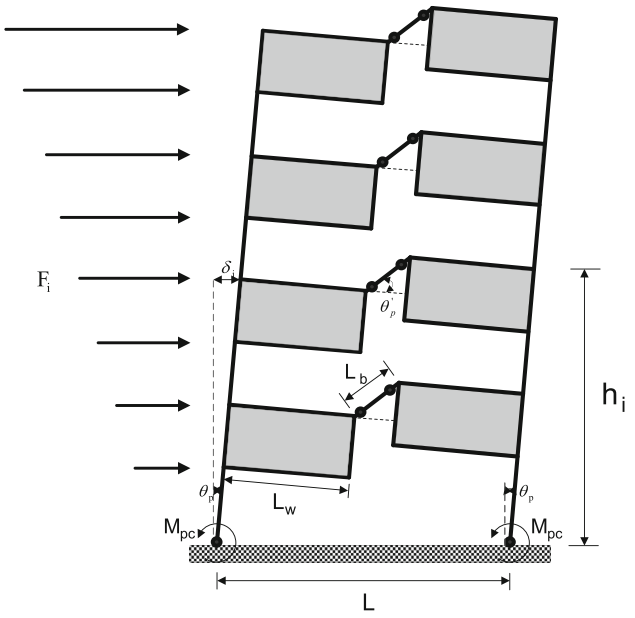

Fig. 12 Desired deformed configuration of the model structure.

equation of the internal and external works (Chao and Goel 2006):

$$\sum_{i=1}^{n} F_i \delta_i = 2M_{pc}\theta_p + 2\sum_{i=2,4,..}^{n} M_{pi}\theta_p' \tag{1}$$

where F_i is the equivalent seismic load obtained using the vertical seismic force distribution method in the ASCE 7-13, $\delta_i = \theta_p h_i$, h_i is the height from the ground to the ith story, M_{pi} is the required plastic moment of the connecting beams in Level i, M_{pc} is the required plastic moment of columns in the first story, L is the length of the transverse side of the structure, L_b is the length of the connecting beam, θ_p is the given target drift, and θ_p' is the rotation of the connecting beam which is $\frac{L}{L_b}\theta_p$. In the above equation the lateral seismic force and the geometric information of the model structure are given values and the moment capacities of the columns and the connecting beams are to be determined. The moment capacity of the first story columns, M_{pc}, can be obtained from the equivalence of the external and internal works assuming that plastic hinges form at the base and the top of the first story columns. In this study the total moment capacity of the connecting beams obtained above is distributed to each story proportional to the seismic story shear as follows:

$$M_{pi} = \frac{\frac{V_i}{V}}{\sum_{i=2,4,...}^{n}\frac{V_i}{V}}\sum_{i=1}^{n} M_{pi} \tag{2}$$

where V_i is the story shear in level i. The connecting beams in each story can be designed using the required moment capacity determined above using a resistance factor specified in the design code. It is expected in this design process that most connecting beams yield when a given lateral drift occurs in the structure.

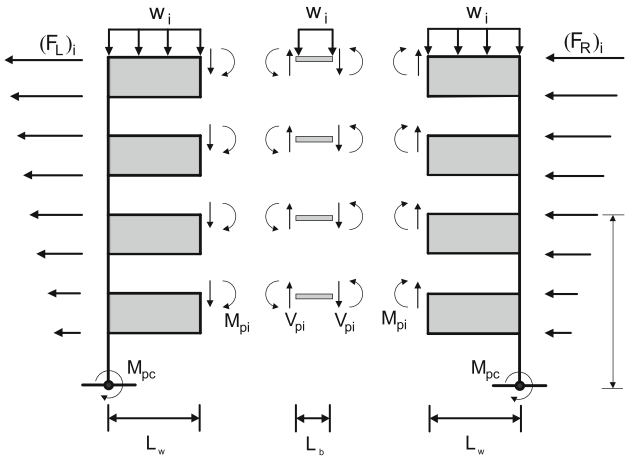

Fig. 13 Free body diagram of the model structure.

the combination of factored gravity loads and the maximum vertical shear force developed at the connecting beams, V_p, which is obtained as follows:

$$V_{pi} = \frac{2R_y M_{pi}}{L_b} = \frac{2(M_{pr})_i}{L_b} \tag{3}$$

where R_y is the overstrength factor of 1.25 recommended in the ACI 318-14 (2011). The required balancing lateral forces applied on the left and right free bodies can be obtained as follows, respectively, using the moment equilibrium:

In this study the total lateral forces obtained above are vertically distributed using the vertical distribution factor specified in the ASCE 7-13. The seismic story forces acting on the left- and right-hand side free bodies used to design the members outside the vierendeel panel are obtained as follows:

$$\sum_{i=1}^{n}(F_L)_i = \frac{\sum_{i=2,4,6...}^{n}(M_{pr})_i + L_w \cdot \sum_{i=2,4,}^{n} V_i + \frac{L_w^2}{2}\cdot\sum_{i=2,4,6...}^{n} w_i + M_{pc}}{\sum_{i=1}^{n} h_i} \tag{4}$$

$$\sum_{i=1}^{n}(F_R)_i = \frac{\sum_{i=2,4,6...}^{n}(M_{pr})_i + L_w \cdot \sum_{i=2,4,6...}^{n} V_i - \frac{L_w^2}{2}\cdot\sum_{i=2,4,6...}^{n} w_i + M_{pc}}{\sum_{i=1}^{n} h_i} \tag{5}$$

Once the beams are designed using the plastic moment obtained in Eq. (2), the next step is to design the exterior columns and staggered walls in such a way that they remain elastic when the connecting beams yield. The staggered walls, which are deep beams with depth of the story height, have significantly large stiffness and bending and shear capacities, and therefore remain elastic at application of design seismic load. Figure 13 shows the free body diagram of a frame of staggered wall structure when all connecting beams yield. To concentrate the plastic hinges at the connecting beams when subjected to seismic load, the elements other than the connecting beams should be designed to resist

$$(F_L)_i = C_{vi}\sum_{i=1}^{n}(F_L)_i \tag{6}$$

$$(F_R)_i = C_{vi}\sum_{i=1}^{n}(F_R)_i \tag{7}$$

The vertical distribution factor at level x, C_{vx}, specified in the ASCE 7-13 is given by

$$C_{vx} = \frac{w_x h_x^k}{\sum_{i=1}^{n} w_i h_i^k} \tag{8}$$

where w_x is the effective seismic weight of the structure at level x, h_x is the height from the base to level x, and k is an exponent related to the structure period. The structural elements other than the connecting beams are designed to respond elastically for the gravity loads and the lateral load computed above. The size and rebars of the first story columns and the second story beams of the structure designed by the capacity design procedure (model CD) are presented in Table 1. It can be observed that the column sizes of the model CD are slightly increased and the longitudinal rebars in the connecting beams are slightly reduced compared with those of the strength designed structure (model SD). According to the eigenvalue analysis results, the fundamental natural period along the transverse direction is 0.41 s, which is almost the same with that of the model SD.

Figure 14 shows the pushover curve of the model CD, in which it can be observed that both the yield and the maximum strengths of the structure are smaller than those of the model SD. As in the model SD, the first yield of the model CD occurs at the 5th story beam. However the major drop of strength occurs as a result of yield of the 4th story beam, and the residual strength is larger than that of the model SD. Figure 15 depicts the maximum inter-story drifts of the model structures at the point of the maximum strength and at the maximum inter-story drift of 2.5% obtained from pushover analysis. It can be noticed that large inter-story drifts occur at mid-height, and the drift patterns of the strength and the capacity-designed structures are similar to each other. Figure 16 depicts the plastic hinge formation in the model structures at the maximum inter-story drift of 2.5% of the story height. It can be observed that, even though the drift patterns are similar to each other, the plastic hinge formations which cause the drift are quite different. In the model SD, most columns are subjected to CP (collapse prevention) level plastic deformation, whereas significant plastic deformations are concentrated in the connecting beams in the model CD. Even though the plastic hinge formation and the failure mode correspond well with those assumed in the design stage of the model CD, significant increase in ductility cannot be achieved due mainly to the insufficient plastic rotation capacity of the beams. In the following section the validities of two different seismic retrofit schemes are investigated for enhancing seismic-load resisting capacity of the staggered wall structure.

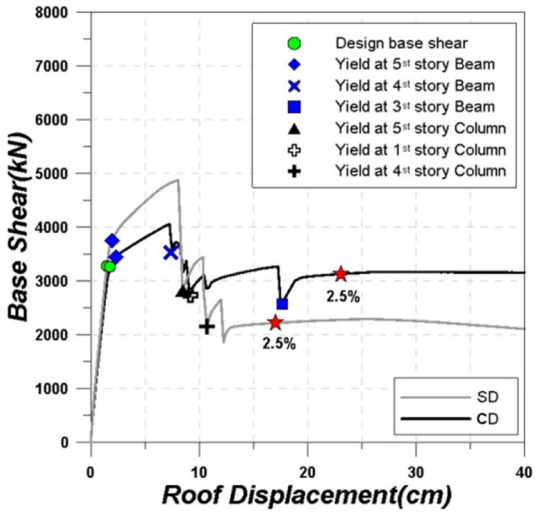

Fig. 14 Pushover curve of the performance-designed structure.

5. Seismic Retrofit Schemes for Staggered Wall Structures

5.1 Addition of Interior Columns

In a typical staggered wall structure, columns exist along the perimeters in the longitudinal direction and the connecting beams are located in alternate floors between two

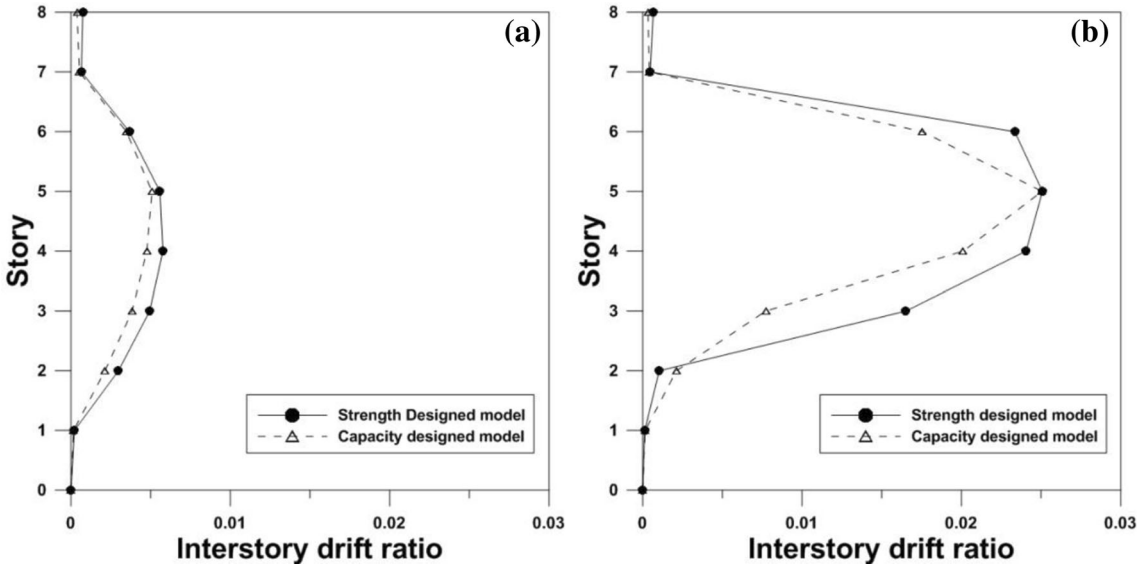

Fig. 15 Maximum inter-story drift ratio of the model structures obtained from pushover analysis. **a** At maximum strength and **b** at maximum inter-story drift of 2.5%.

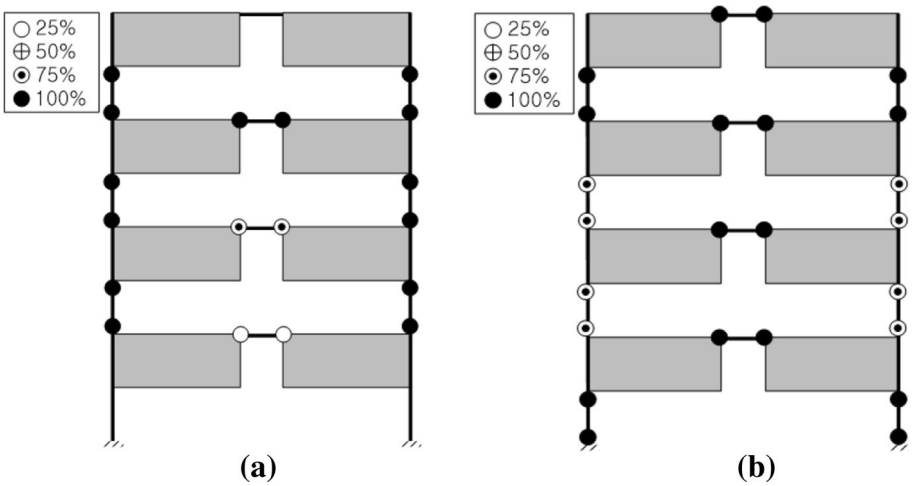

Fig. 16 Plastic hinge formation in the model structures at the maximum inter-story drift ratio of 2.5%. **a** Strength-designed model and **b** capacity designed model.

staggered walls. As a means of enhancing seismic load resisting capacity of the system, internal columns with 200 × 600 mm in cross section reinforced with 4-D19 rebars are added along the corridor. In the stories where staggered walls exist, the internal end of the wall is reinforced as a column. The internal columns are continuous from the second to the top stories, and are designed to resist only seismic load. In the structure with interior columns, connecting beams can be placed in every story between the internal columns. Figure 17 shows the structural plan and elevation of the analysis model structure with interior columns (model CD_IC). The same capacity design procedure applied previously to design the model CD is applied to the design of the retrofitted structure with internal columns. The energy equilibrium equation applied in this model is similar to that of the original model, except that the deformation of each connecting beam located every story contributes to the internal work as follows:

$$\sum_{i=1}^{n} F_i \delta_i = 2M_{pc}\theta_p + 2\sum_{i=1,2,..}^{n} M_{pi}\theta_p' \tag{9}$$

Also the required balancing lateral forces, obtained similarly to Eqs. (4) and (5) considering the plastic moments of the added connecting beams, are applied to the design of the interior as well as the exterior columns. The member sizes of the model structure with interior columns are presented in Table 1, where it can be observed that both the column size and the beam rebars decrease as a result of the addition of interior columns. The fundamental natural period along the transverse direction is reduced to 0.31 s due to the increased stiffness.

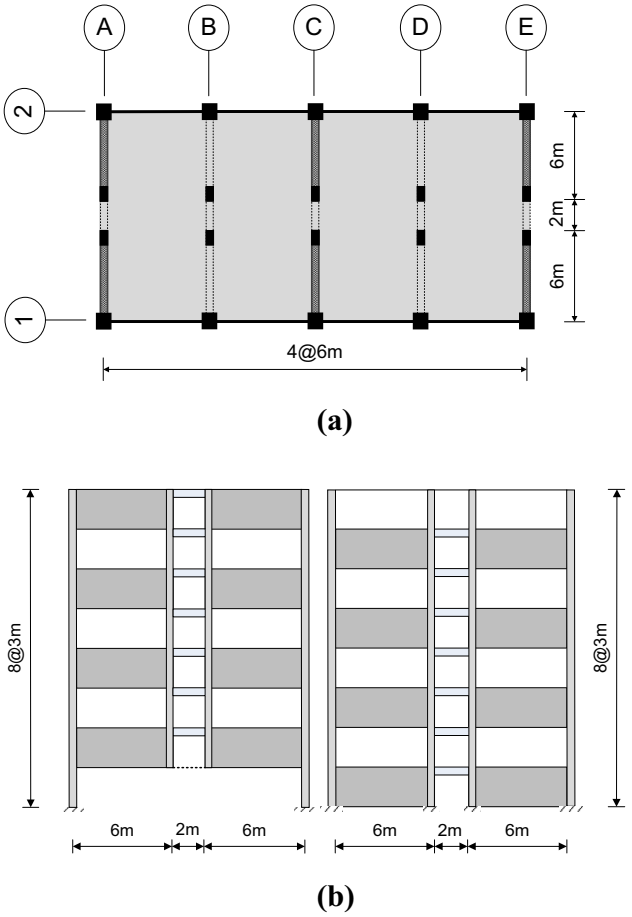

Fig. 17 Analysis model structure with interior columns. **a** Structural plan and **b** structural elevation.

5.2 Addition of Rotational Friction Dampers

In the second retrofit scheme, rotational friction dampers are installed at the ends of connecting beams as shown in Fig. 18a. Figure 18b depicts the bending moment–rotation relationship of a typical rotational friction damper. The insertion of rotational friction dampers significantly increases the rotational capacity of the connecting beams. Rotational friction dampers can be manufactured to have larger deformation and energy dissipation capacity than those of typical plastic hinges formed at beam ends. They also can be reused after experiencing small to medium earthquakes. The effectiveness of the friction dampers has been verified by many researchers. Morgen and Kurama (2008) carried out a seismic response evaluation tests of

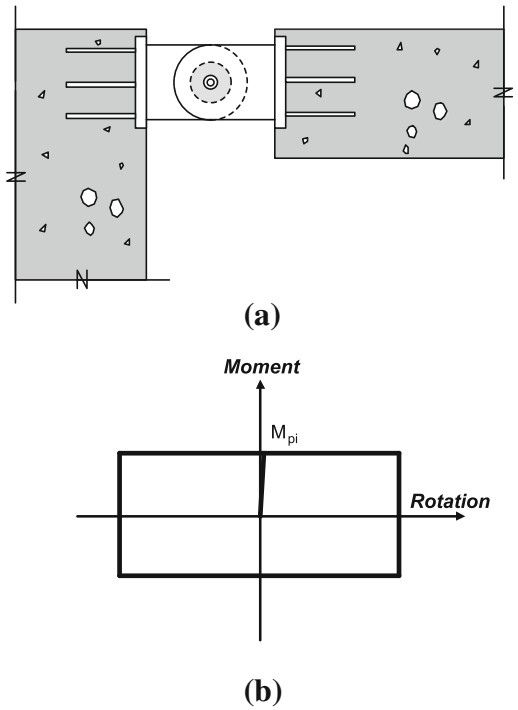

Fig. 18 Rotational friction damper considered in this study. **a** Installed configuration between staggered wall and connecting beam and **b** moment–rotation relationship.

Table 2 Member size and rebars of the second story coupling beams in the frame A.

Model	Longitudinal bar	
	Top	Bottom
SD	5-D22	5-D22
CD, CD_FD	5-D13	5-D13
CD_IC	2-D19	2-D19

unbonded posttensioned precast concrete moment frames with friction dampers at selected beam ends. Mualla et al. (2010) developed a rotational friction damper which can produce maximum friction force as high as 5000 kN (Table 2).

For model structures with rotational friction dampers at the ends of connecting beams, the same capacity design procedure is applied to lead the formation of plastic hinges in the connecting beams where the friction dampers are installed. The slip forces of the dampers are determined in such a way that their moment capacities are equal to the maximum moment of the connecting beams. To ensure yielding of dampers prior to other structural elements when the model structure is subjected to design seismic load, the structures are designed in such a way that the plastic hinges are concentrated at the connecting beams and the other members remain elastic. The failure point of the friction dampers at which the friction force is lost is conservatively assumed to be 0.3 rad based on the experimental results of rotational friction dampers (Chung et al. 2009).

5.3 Seismic Performance of the Retrofitted Structures

Figure 19 shows the pushover curves of the model structure retrofitted with the two schemes described above. The pushover curve of the performance or capacity-designed structure (model CD) is also presented for comparison. The pushover curve of the structure with interior columns (model CD_IC) is presented in Fig. 19a, where it is observed that the maximum strength is significantly increased due to the addition of the interior columns. The roof displacement at the maximum inter-story drift of 2.5% is larger than that of the model CD, which is more desirable in the sense that plastic damage is not concentrated in a few stories but is more uniformly distributed. Figure 19b depicts the pushover curve of the model with friction dampers at beam ends (CD_FD). It can be observed that, as the yield moments of the friction dampers are equal to those of the beam ends of the model CD, the yield strengths of the two models are similar to each other. However, as the rotational capacity of the friction dampers is much larger than that of the connection beams, ductility is significantly increased compared with the model CD. The increase in the roof displacement at

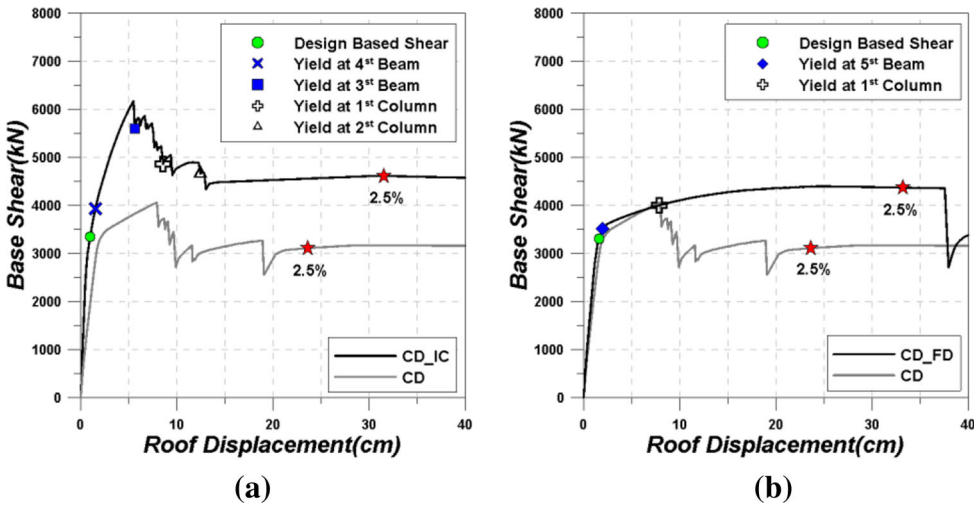

Fig. 19 Pushover curves of the retrofitted staggered wall structures. **a** Model CD_IC and **b** Model CD_FD.

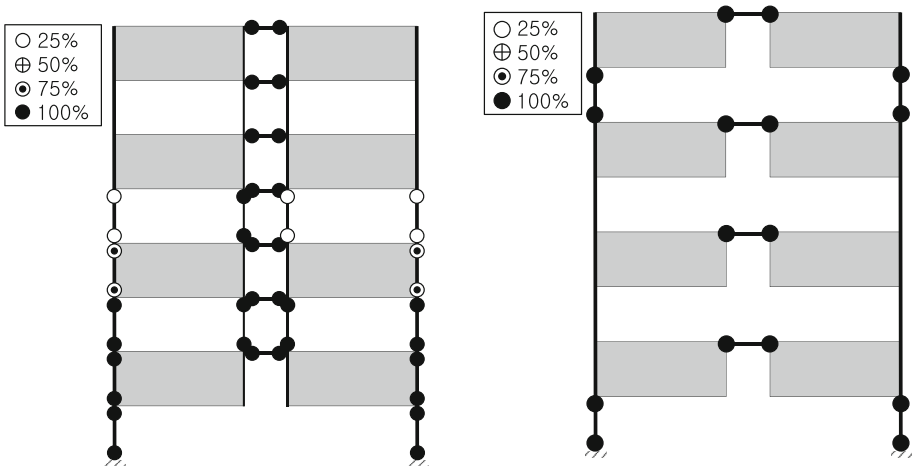

Fig. 20 Plastic hinge formation in the structure with friction dampers. **a** Model CD_IC and **b** Model CD_FD.

the maximum inter-story drift of 2.5% is also significant compared with that of the model CD. Figure 20 shows the plastic hinge formation in the retrofitted structures at the maximum inter-story drift of 2% of the story height. It can be observed that most connecting beams yield as assumed in the design process. However in the model CD_IC many plastic hinges also form in the exterior and interior columns, which results in sharp drop of strength compared with the behavior of the model with friction dampers.

Figure 21 compares the hysteretic energy dissipated by each structural element obtained by nonlinear dynamic analysis of the models CD_IC and CD_FD using the Northridge earthquake ground motion. It can be noticed that the hysteretic energy dissipated in the beams of the model CD_IC is only 93% of the total hysteretic energy, whereas about 99% of the hysteretic energy is dissipated in the friction dampers in the model CD_FD. This implies that most structural elements are free from any damage during the earthquake. It also can be observed that the total hysteretic energy is significantly smaller in the model CD_IC due to the increased redundancy and decreased plastic deformation.

6. Seismic Safety of the Model Structures

6.1 Collapse Margin of the Model Structures

In this section the validity of the capacity design approach and the retrofit schemes for staggered wall structures is verified by statistical seismic performance evaluation procedure proposed in the FEMA P695 (2009). In this approach nonlinear incremental dynamic analyses are conducted to establish the median collapse capacity and collapse margin ratio (*CMR*) for the analysis models. The adjusted collapse margin ratio (ACMR) is obtained by multiplying the collapse margin ratio (*CMR*), which is the ratio of the median collapse intensity ($\widehat{S_{CT}}$) and the MCE (maximum considered earthquake) intensity (S_{MT}), and the spectral shape factor. Acceptable values of adjusted collapse margin ratio are based on total system collapse uncertainty, β_{TOT}, and established values of acceptable probabilities of collapse.

To evaluate the seismic performance of the model structures following the FEMA P695 process, incremental dynamic analyses of the model structures are carried out using the 22 pairs of scaled far-field records provided by the PEER NGA Database (2006). The general procedure for incremental

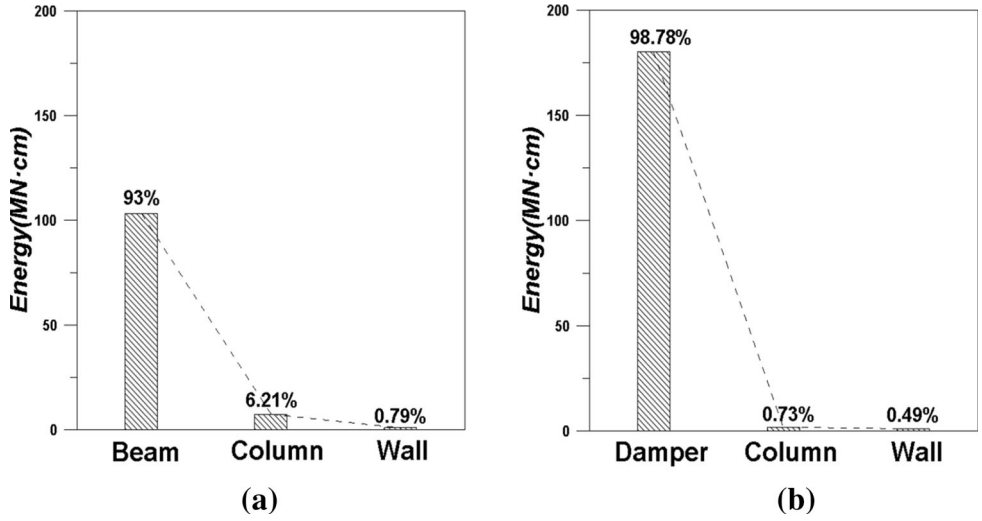

Fig. 21 Hysteretic energy dissipated by each structural element. **a** CD_IC and **b** CD_FD.

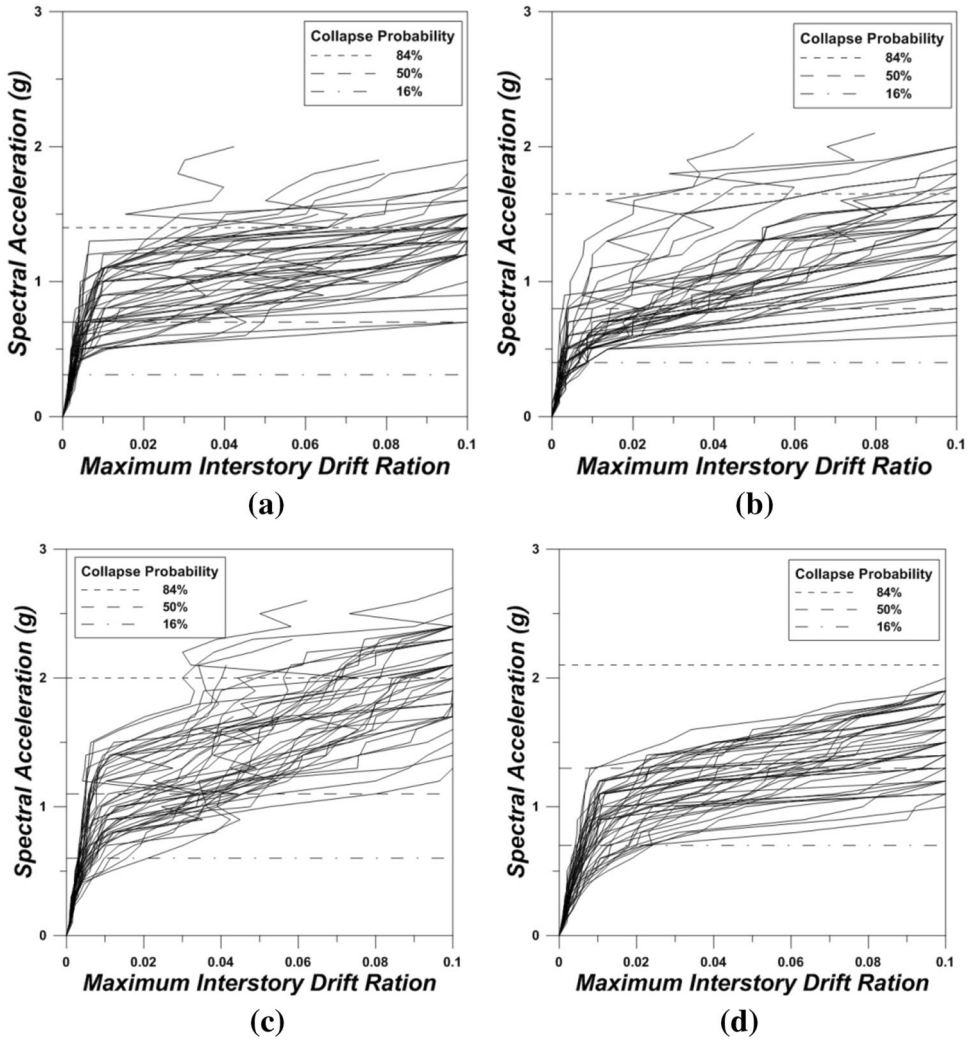

Fig. 22 Incremental dynamic analysis curves of the analysis model structures. **a** SD($\widehat{S_{CT}} = 0.7$), **b** CD($\widehat{S_{CT}} = 0.8$), **c** CD_IC($\widehat{S_{CT}} = 1.1$), and **d** CD_FD($\widehat{S_{CT}} = 1.3$).

Table 3 Estimation of collapse margin of the model structures.

	$\widehat{S}_{CT}$	S_{MT}	*CMR*	*SSF*	*ACMR*	$ACMR_{20\%}$	Pass/fail
SD	0.7	0.25	2.8	1.08	3.1	1.8	Pass
CD	0.8	0.24	3.3	1.09	3.5	1.8	Pass
CD_IC	1.1	0.25	4.4	1.08	4.7	1.8	Pass
CD_FD	1.3	0.24	5.4	1.14	6.1	1.8	Pass

dynamic analysis is well documented in Vamvatsikos and Cornell (2002). Figure 22 depicts the incremental dynamic analysis results of the model structures using the 44 earthquake records. The collapse margin ratios (CMR) of the model structures are obtained from the spectral accelerations at which dynamic instability of the structures occurred for more than 22 earthquake records. The spectral accelerations corresponding to the 16, 50, and 84% of failure probability are indicated in the IDA curves. It can be observed that the median collapse intensity ($\widehat{S_{CT}}$), which is the 50% probability of failure, increases in the retrofitted structures. Especially the capacity-designed structure with rotational friction dampers (model CD_FD) shows the largest median collapse intensity. Similar trend can be observed in the other failure probabilities. In this study the total system collapse uncertainty is evaluated as 0.7 in accordance with Table 7-2 of FEMA P695. Table 3 shows all parameter values used in the computation of the adjusted collapse margin ratios of all model structures obtained from the incremental dynamic analysis results. It can be observed that the adjusted collapse margin ratios (ACMR) of all model structures are larger than the acceptable values of *ACMR* 20% provided in the FEMA P695 and the parameters used in the seismic design of the model structures are valid. It also can be noticed that the collapse margin of the model structure designed with friction dampers, model CD_FD, is significantly larger than those of the other model structures.

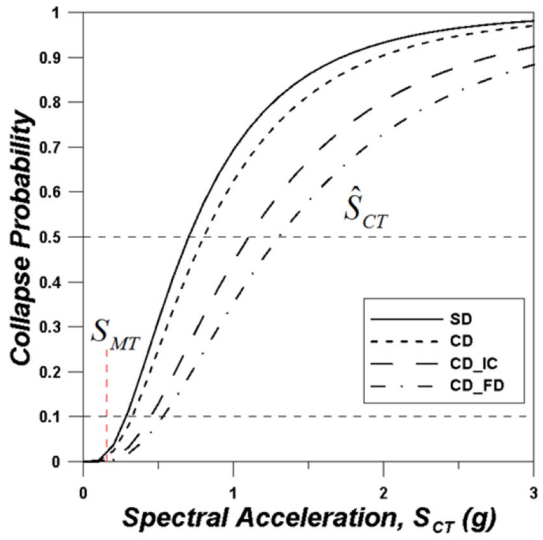

Fig. 23 Fragility curves of the model structures for reaching the state of dynamic instability.

6.2 Fragility Analysis

Fragility analysis is carried out to investigate the failure probability of each model structure for a given seismic intensity. The seismic fragility is described by the conditional probability that the structural capacity, C, fails to resist the structural demand, D, given the seismic intensity hazard and is modeled by a lognormal cumulative distribution function as follows (Cornell et al. 2002):

$$\mathrm{P}[\mathrm{D} \geq \mathrm{C}] = \Phi(\ln[D/\hat{C}]/\beta_c) \tag{10}$$

where $\Phi[\cdot]$ = Standard normal probability integral, $\hat{C}$ = median structural capacity associated with the limit state, and β_C = uncertainty in C. In this study the median structural capacity is obtained from the incremental dynamic analysis results of the model structures, and the fragility for a given spectral acceleration is computed from Eq. (10) using the total system collapse uncertainty of 0.7. The state of dynamic instability is considered as the failure state, at which the stiffness decreases lower than 20% of the initial stiffness in the incremental dynamic analysis.

Figure 23 depicts the probability of reaching the failure state, where it can be observed that, for the same spectral acceleration, the collapse probability is highest in the strength designed structure (model SD) and is lowest in the structure with friction dampers (model CD_FD). The

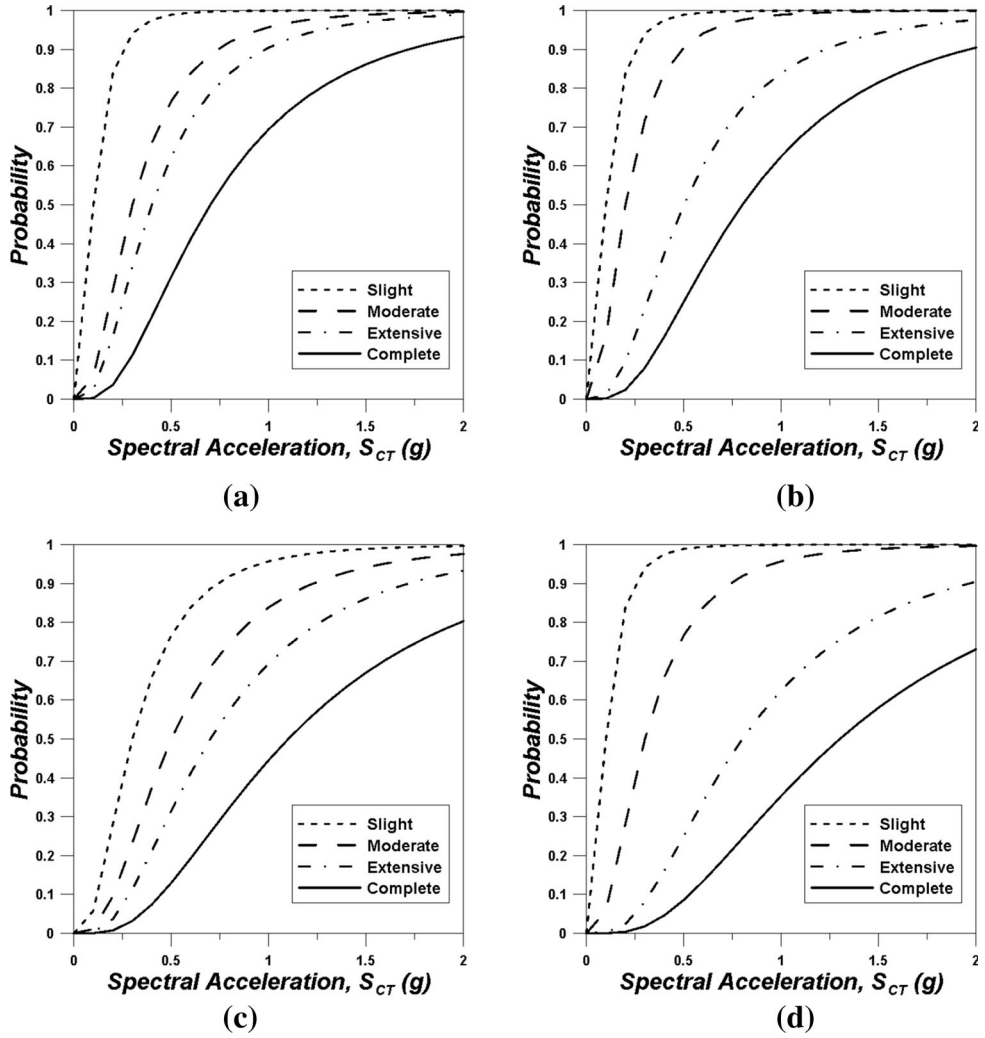

Fig. 24 Fragility curves of the model structures for reaching the four damage states. **a** Model SD, **b** Model CD, **c** Model CD_IC, and **d** Model CD_FD.

spectral acceleration at the 50% probability of failure (dynamic instability) is 0.7 and 1.3 g, respectively, for the model SD and CD_FD. FEMA P695 requires that the probability of failure of a structure corresponding to the MCE level earthquake, which is 3/2 of the design level spectral acceleration, be smaller than 0.1 so that the seismic design variables used for the model structures are valid. This condition is satisfied in all model structures and therefore it can be concluded that the response modification factor of 3.0 is valid in the seismic design of the staggered wall structure.

Fragility analyses are also carried out for the four damage states defined in the HAZUS (2010), which are Slight, Moderate, Extensive, and Complete damage. The Complete damage state is defined as the maximum inter-story displacement at which the strength decreases to 80% of the maximum strength in the pushover curve. The states of the Slight damage and the Moderate damage were defined as the spectral displacements corresponding to the 70 and the 100% of the yield point, respectively. The Extensive Damage was defined as the quarter point from the Moderate to the Complete damage. Figure 24 depicts the fragility curves of the analysis model structures, where it can be observed that the structures designed with friction dampers have significantly lower probability of reaching the collapse state than the strength-designed structure. It can be observed that the probability of the model CD to reach the Moderate damage state is slightly larger than that of the model SD. However those to reach the Extensive and the Complete damage states are somewhat decreased. This implies that the capacity design applied in this study is only effective for large earthquakes which cause severe damage to structures. In the model CD_IC the probabilities of reaching the Slight and the Moderate damage states are somewhat lower than those of the other models, and those of reaching the Extensive and the Complete damage states are between the models SD/CD and the CD_FD. The probabilities of the model CD_FD to reach the Slight and the Moderate damage states are similar to those of the model SD. However decrease in the probabilities of reaching the Extensive and the Complete damage states are most significant in this model.

Table 4 Member size and rebars of the first story exterior columns designed using R = 5.

Model	Frame	Size (mm)	Main bar
SD	A	460 × 460	8-D25
	B	580 × 580	8-D25
CD	A	480 × 480	8D-29
	B	580 × 580	8D-29
CD_IC	A	480 × 480	8D-29
	B	560 × 560	8D-29
CD_FD	A	480 × 480	8D-29
	B	580 × 580	8D-29

7. Response of Structures Designed with Higher R Factor

It is observed in the previous section that both the standard and the retrofitted model structures designed using the response modification (R) factor of 3 satisfy the FEMA P695 requirements. In this section all model structures are redesigned with increased R factor of 5 (i.e. with reduced seismic load) and their seismic performances are compared with those of the structures designed with R = 3. Tables 4 and 5 show the size and rebars of the selected members in the structure designed using R=5. Figure 25 shows the pushover curves of the model structures designed with reduced seismic load, where it can be observed that the overall strengths of all model structures are significantly reduced as a result of using increased R factor. The strength of the model structure

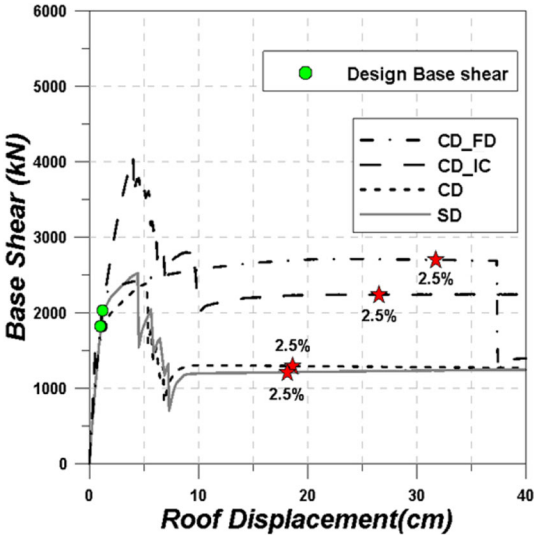

Fig. 25 Pushover curves of the model structures designed using R = 5.

Table 5 Member size and rebars of the second story coupling beams in the frame A designed using R = 5.

Model	Longitudinal bar	
	Top	Bottom
SD	3-D19	3-D19
CD, CD_FD	2-D19	2-D19
CD_IC	2-D16	2-D16

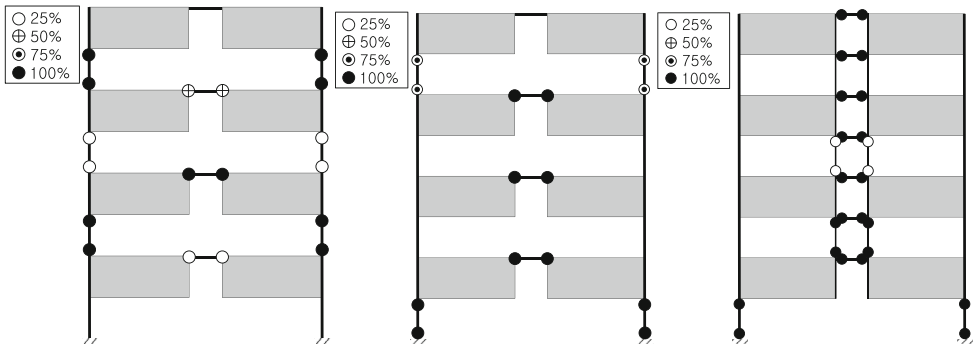

Fig. 26 Plastic hinge formation in the structures designed using R = 5. **a** SD, **b** CD, and **c** CD_IC.

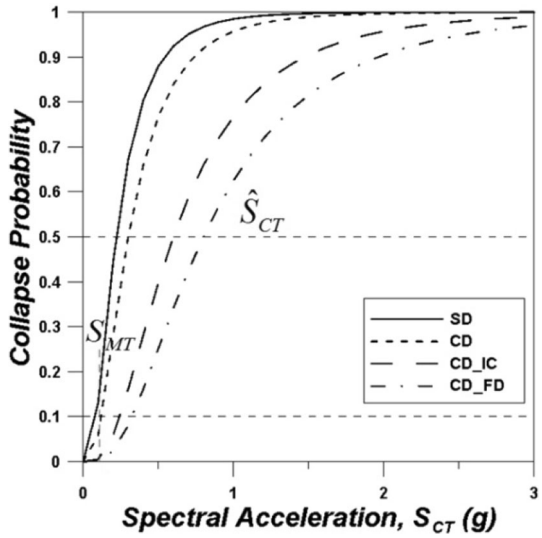

Fig. 27 Fragility curves of the structures designed using R = 5 for reaching dynamic instability.

with interior columns is the highest among the all model structures, and the ductility is highest in the structure with friction dampers. As observed in the previous sections, the major strength drop of the strength-designed model SD occurs due to plastic hinges in the exterior columns whereas the other structures designed by capacity design process fail by concentration of plastic hinges in beams. These observations can be verified by the plastic hinge formations at the maximum inter-story drift of 2.0% presented in Fig. 26, where it can be noticed that the plastic hinge formations of the redesigned structures are quite similar to those of the structures designed using R = 3 except the fact that plastic hinges are more concentrated in the connecting beams in the model CD_IC. The plastic hinge formation in the model CD_FD is the same with that of the model CD.

Figure 27 depicts the fragility curves of the four model structures obtained from incremental dynamic analyses using the 44 earthquake records. Compared with the fragility curves of the model structures designed with R = 3 shown in Fig. 23, the collapse probabilities are significantly increased in the structures designed using R = 5. It can be noticed that the collapse probabilities of the models SD and CD exceed 0.1 which is the limit state specified in the FEMA P 695 to validate the seismic design parameters used, while those of the retrofitted structures are still far below the limitation. Therefore based on the analysis results it can be concluded that the structures retrofitted with interior columns or friction dampers may be designed using higher R factor than 3.0.

8. Conclusions

This study investigated the seismic performance of a staggered wall structure designed with conventional strength based design, and compared it with the performance of the structures designed by capacity design procedure. Then the seismic reinforcement schemes such as addition of interior columns or insertion of rotational friction dampers at the ends of connecting beams were validated by comparing their seismic performances with those of the standard model structure.

According to pushover analysis, the strength-designed structure failed due mainly to failure of exterior columns, whereas in the capacity designed structures major strength drop occurred due to plastic hinge formation in beams. Fragility analysis showed that the probability to reach the dynamic instability was highest in the strength designed structure and was lowest in the structure with friction dampers. The capacity design applied in this study turned out to be most effective for large earthquakes which cause severe damage to structures. In the model with interior columns, the probabilities of reaching the Slight and the Moderate damage states were quite significant, and the probability of reaching the Extensive and the Complete damage states decreased most substantially in the structure with friction dampers. The collapse probabilities of all model structures designed with the R factor of 3.0 were smaller than 0.1, which confirmed that the seismic design variables used for the model structures were valid. However in the structures designed with the R factor of 5.0, the collapse probabilities turned out to be less than 0.1 only in the structures retrofitted with interior columns or friction dampers. Based on the analysis results of the specific analysis model structures considered in this study, it was concluded that R factor of 5.0 might be used in the seismic design of staggered wall structures with proposed retrofit schemes, while R factor of 3.0 might be reasonable for standard staggered wall structures.

Acknowledgements

This paper was supported by Sungkyun Research Fund, Sungkyunkwan University, 2016.

References

ACI 318. (2014). *Building code requirements for structural concrete (318-14) and commentary*. Farmington Hills, MI: American Concrete Institute.

AISC. (2010). *Seismic provisions for structural steel buildings, AISC 341-10*. Chicago: American Institute of Steel Construction.

ASCE 41-13. (2013). *Seismic Rehabilitation of Existing Buildings*. Reston: American Society of Civil Engineers.

ASCE 7-13. (2013). *Minimum design loads for buildings and other structures*. Reston: American Society of Civil Engineers.

ATC-19. (1995). *Structural response modification factors*. Redwood City, CA: Applied Technology Council.

Chao, S.-H., & Goel, S. C. (2006). *Performance-Based Plastic Design of Seismic Resistant Special Truss Moment Frames*. Report No. UMCEE 06-03. Department of Civil and Environmental Engineering, University of Michigan, Ann Arbor, MI.

Chung, H., Moon, B., Lee, S., Park, J., & Min, K. (2009). Seismic performance of friction dampers using flexure of RC shear wall system. *The Structural Design of Tall and Special Buildings, 18,* 807–822.

Cornell, C. A., Jalayer, F., Hamburger, R. O., & Foutch, D. A. (2002). The probabilistic basis for the 2000 SAC/FEMA steel moment frame guidelines. *ASCE Journal of Structural Engineering, 128*(4), 526–533.

FEMA P695. (2009). *Quantification of building seismic performance factors*. Washington, DC: Federal Emergency Management Agency.

Fintel, M. (1968). Staggered transverse wall beams for multistory concrete buildings. *ACI Journal, 65*(5), 366–378.

HAZUS-MH 2.1. (2010). *Technical Manual Washington*. Washington, DC: Federal Emergency Management Agency.

Kang, J., Yoon, H., Kim, W., Kodur, V., Shin, Y., & Kim, H. (2016). Effect of wall thickness on thermal behaviors of RC walls under fire conditions. *International Journal of Concrete Structures and Materials, 10,* 19–31.

Kim, D. K. (2016). Seismic response analysis of reinforced concrete wall structure using macro model international journal of concrete. *Structures and Materials, 10*(1), 99–112.

Kim, J., & Baek, D. (2013). Seismic risk assessment of staggered wall system structures. *Earthquake and Structures, 5,* 607–624.

Kim, J., Jun, Y., & Kang, H. (2016). Seismic behavior factors of RC staggered wall buildings. *International Journal of Concrete Structures and Materials, 10*(3), 355–371.

Kim, J., & Kim, S. (2017). Performance-based seismic design of staggered truss frames with friction dampers. *Thin-Walled Structures, 111,* 197–209.

Kim, J., & Lee, M. (2014). Fundamental period formulae for RC staggered wall buildings. *Magazine of Concrete Research, 66*(7), 325–338.

Kim, J., Lee, J., & Kim, B. (2015). Seismic retrofit schemes for staggered truss structures. *Engineering Structures, 102*(1), 93–107.

Lee, J., & Kim, J. (2013). Seismic performance evaluation of staggered wall structures using FEMA P695 procedure. *Magazine of Concrete Research, 65*(17), 1023–1033.

Lee, J., & Kim, J. (2015). Seismic response modification factors of reinforced concrete staggered wall structures. *Magazine of Concrete Research, 67*(20), 1070–1083.

MacKay-Lyons, R. (2013). *Performance-based design of RC coupled wall high-rise buildings with viscoelastic coupling dampers*. Master's thesis, Department of Civil Engineering, University of Toronto.

Madsen, L. P. B., Thambiratnam, D. P., & Perera, N. J. (2003). Seismic response of building structures with dampers in shear walls. *Computers & Structures, 81*(4), 239–253.

Mao, C. X., Wang, Z. Y., Zhang, L. Q., & Li, H. (2012). Seismic performance of RC frame-shear wall structure with novel shape memory alloy dampers in coupling beams. In *15th World congress of earthquake engineering (15 WCEE)*, Lisbon, Portugal.

Mee, A. L., Jordaan, I. J., & Ward, M. A. (1975). Dynamic response of a staggered wall-beam structure. *Earthquake Engineering and Structural Dynamics, 3*(4), 353–364.

Morgen, B. G., & Kurama, Y. C. (2008). Seismic response evaluation of posttensioned precast concrete frames with friction dampers. *Journal of Structural Engineering, 134*(1), 132–145.

Mualla, I. H., Jakupsson, E. D., & Nielsen, L. O. (2010). Structural behavior of 5000 kN damper. In *European conference on earthquake engineering*, ECEE, Ohrid, Macedonia.

PEER, NGA Database. (2006). Pacific Earthquake Engineering Research Center, University of California, Berkeley. http://peer.berkeley.edu/nga.

Pant, D. R., Montgomery, M., Berahman, F., & Christopoulos, C. (2015). Resilient seismic design of tall coupled shear wall buildings using viscoelastic coupling dampers. In *11th Canadian conference on earthquake engineering (11CCEE)*, Victoria, Canada.

Paulay, T., & Priestley, M. J. N. (1992). *Seismic design of reinforced concrete and masonry building*. New York: Wiley.

PERFORM-3D. (2006). *Nonlinear analysis and performance assessment for 3D structures-user guide*. Berkeley, CA, USA: Computers and Structures.

Vamvatsikos, D., & Cornell, C. A. (2002). Incremental dynamic analysis. *Earthquake Engineering and Structural Dynamics, 31*(3), 491–514.

Wallace, J. W. (2012). Behavior, design, and modeling of structural walls and coupling beams—Lessons from recent laboratory tests and earthquakes. *International Journal of Concrete Structures and Materials, 6*(1), 3–18.